Inverter Controller with Synthetic Inertia and Adaptive Harmonic Damping Based on Fourier Linear Combiners

Thiago Silva Amorim, Odair de Barros Junior, Daniel Carletti, Lucas Frizera Encarnação

***Abstract*—This paper proposes an inverter control strategy that combines virtual synchronous generator control with harmonic detection based on Fourier linear combiners with adaptive gain. In the proposed strategy, the virtual synchronous generator control calculates the current in the fundamental frequency component, responsible for the control inertial characteristic, and harmonic voltage detector based on Fourier linear combiners selectively detects the harmonic voltages to be damped. The 5th harmonic order adaptive gain is calculated from voltage and current measurements on a bus of interest in the system. Real-time simulation results were developed in a hardware-in-the-loop test-bench to show that the proposed control can simultaneously mitigate the grid voltage and current harmonics and reduce the peaks of frequency oscillations after transients.**

***Keywords*: distributed generation, Fourier linear combiner, harmonic detection, power quality, virtual synchronous generator.**

I. Introduction

TECHNOLOGICAL innovations and changes in the regulatory environment have led to the growing presence of distributed generation (DG) units in the electrical system, such as photovoltaic panels. However, some DG units do not provide inertia to support the grid frequency stability [1]. The virtual synchronous generator (VSG) is proposed as a control strategy for DC-AC converters to emulate the inertial behavior and electromechanical oscillations damping nature of synchronous machines [2]. As well as the growth of DG units in the electrical system, the proliferation of devices based on power electronics, that consume harmonic currents, can deteriorate the electrical system power quality. The application of active power filters (APF) is an alternative to mitigate the harmonics present in the electrical system [3]. As VSG and APF controls are applied on DC-AC converters, it is possible to embed both controls in a single inverter.

Some authors have proposed works that combine the functionality of VSGs with harmonic compensation, which seek to simultaneously improve system stability and mitigate voltage distortions and harmonic currents present in an electrical system. In [4], the authors propose the application of the VSG control combined with a harmonic detector based on the synchronous reference system (Park Transform) in a three-phase four legs inverter. In [5], the authors propose an inverter control that combines VSG strategy and amended fractional order repetitive control (AFORC). In [6], the authors compare the combination of VSG control with three harmonic detection strategies based on the instantaneous power theory (*p*-*q* Theory), highlighting the pros and cons of each harmonic detection strategy. In [7], the authors propose the combination of VSG control with a hybrid harmonic suppression strategy to simultaneously eliminate the distortions of the inverter's local voltage and the power grid current. Harmonic detection is done through the multiple harmonic sequence components observer (MHSCO). In [8], the authors propose the Synchronfilter, the combination of an active filter operating with the virtual inertia functionality based on the control of a Synchronverter, with selective harmonic detection performed through proportional-resonant controllers. In [9], the authors propose the combination of VSG control with a harmonic voltage reduction strategy based on harmonic VSG that selectively mitigates voltage harmonics. In addition to adding inertial characteristics to the fundamental component of the current, this strategy also adds inertial characteristics to the compensating harmonic currents. Among the works presented, [7]-[9] selectively detect the harmonic orders to be compensated. The emulated electrical systems of the works presented in [4]-[9] are quite limited, with only two buses, one in which the system voltage source and another in which the loads and the DG unit are connected. This system limitation restricts these works' contributions, i.e. making it impossible to visualize the system's interaction with multiple DGs.

This work proposes an inverter control strategy that combines VSG control with harmonic detection based on Linear Fourier Combiners (FLC) with adaptive gain. The proposed strategy has internal and global control loops using local and system measurements, respectively. This arrangement enables the interaction of multiple DGs with a minimum of global information.

Fig. 1 shows the proposed control strategy that combines VSG control with a harmonic detection strategy based on

This work was supported by National Council for Scientific and Technological Development – CNPq (grant numbers 409024/2021-0 and 311848/2021-4) and Espírito Santo Research and Innovation Support Foundation – FAPES (grant numbers 514/2021, 668/2022 and 1024/2022).

T. S. Amorim is with Federal University of Espírito Santo, Vitória, ES 29075910 Brazil (e-mail of corresponding author: t.s.amorim@hotmail.com).
O. Barros Jr. is with Federal University of Espírito Santo, Vitória, ES 29075910 Brazil (e-mail: ojbarros@gmail.com).
D. Carletti is with Federal University of Espírito Santo, Vitória, ES 29075910 Brazil (e-mail: danielc.ufes@gmail.com).
L. F. Encarnação is with Federal University of Espírito Santo, Vitória, ES 29075910 Brazil (e-mail: lucas.encarnacao@ufes.br).

Paper submitted to the International Conference on Power Systems Transients (IPST2023) in Thessaloniki, Greece, June 12-15, 2023.

FLC. This strategy provides synthetic inertia for the system fundamental component of the current and selectively compensates for the 5th, 7th, 11th, and 13th harmonic orders. Harmonic compensation is selective in both sequence and harmonic order, with a k_{v5} adaptive gain for the 5th order, a k_{v7} gain for the 7th order, a k_{v11} gain for the 11th, and a k_{v13} gain for the 13th harmonic order. The adaptive gain is updated from measurements of the amplitude of 5th harmonic order currents and voltages of a bus of interest ($GRID_{Bus}$). Harmonic voltage detection on the DG bus (DG_{Bus}) is done using three-phase weighted-frequency Fourier linear combiner / sequence detector Fourier linear combiner (3WFLC/SDFLC), which measures only the voltage at the DG_{Bus} to detect voltage harmonics, and the amplitude of 5th harmonic voltages and currents on $GRID_{Bus}$ are done using three-phase weighted-frequency Fourier linear combiner / Fourier linear combiner (3WFLC/FLC). The global external loop is updated every 0.2 s (T_u) and the sampling time (T_s) of the DG unit control internal loop is 0.1 ms.

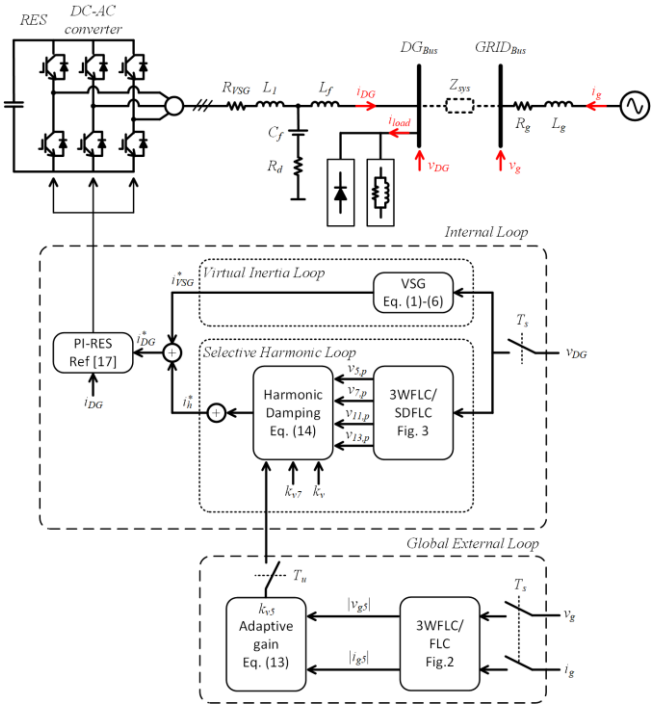

Fig. 1 - Overview of an application of the VSG control with harmonic detection FLC-based with adaptive gain

II. Virtual Synchronous Generator

The VSG model used in this work is based on the model presented in [10]. A three-phase synchronous machine (SM) model is used to calculate the reference currents. The three-phase model reproduces the SM stator circuit and the mechanical subsystem. In place of a field circuit, an induced voltage in the stator is considered.

Equations (1) and (2) describe the rotor electromechanical dynamics [11].

$$T_m - T_e - D \cdot \Delta\omega = \frac{P_m}{\omega} - \frac{P_e}{\omega} - D \cdot \Delta\omega = J\frac{d\omega}{dt} \quad (1)$$

$$\frac{d\theta}{dt} = \omega \quad (2)$$

Where T_m is the mechanical torque, T_e is the electrical torque, P_m is the mechanical power, P_e is the electrical power, ω is the angular velocity, Δ_ω is the angular velocity deviation, θ is the rotor angle, D is the damping factor, and J is the virtual moment of inertia.

The inverter can respond to frequency variations in the system like a synchronous machine with the addition of mechanical equations (1) and (2) in active power control [2].

The VSG current reference can be represented in the Laplace domain, as shown in (3).

$$\vec{i}^*_{VSG} = (\vec{e} - \vec{v}_{DG})/(R_{VSG} + L_{VSG} \cdot s) \quad (3)$$

Where $\vec{e} = [e_a \quad e_b \quad e_c]^T$ is the induced electromotive force (EMF) at stator windings, $v_{DG} = [v_a \quad v_b \quad v_c]^T$ is the voltage at the DG point of common coupling (PCC), $\vec{i}^*_{VSG} = [i_a \quad i_b \quad i_c]^T$ is the VSG current reference, R_{VSG} is the stator virtual resistance, and L_{VSG} is the stator virtual inductance, which in this work is chosen to be to the value of series association of the LCL filter inductances L_1 em L_f.

The induced EMF amplitude is given by (4) and (5). If the control aims to regulate the voltage at the PCC, (4) should be used. if the control aims to control the reactive power supplied by the inverter to the system, (5) should be used.

$$E_p = E^* + (V^* - V)\left(K_{pVVSG} + K_{iVVSG}/s\right) \quad (4)$$

$$E_p = E^* + (Q^* - Q)\left(K_{pQVSG} + K_{iQVSG}/s\right) \quad (5)$$

Where E^* is the induced EMF reference, V^* is the reference peak voltage at the PCC, V is the peak VSG output voltage, K_{pVVSG} and K_{iVVSG} is the voltage controller proportional and integral gains, respectively, Q^* is the reference inverter reactive power, Q is the inverter reactive power, and K_{pQVSG} and K_{iQVSG} is the voltage controller proportional and integral gains, respectively.

The VSG-induced EFM is shown in (6).

$$\vec{e} = E_p[\sin(\theta) \quad \sin(\theta - 2\pi/3) \quad \sin(\theta + 2\pi/3)]^T \quad (6)$$

Simplifications of the three-phase model of the SM result in the lack of transient and subtransient components of the stator current [10].

III. Fourier Linear Combiner

The use of FLC is an alternative to detect the fundamental and harmonic components of a periodic signal. The FLC is based on the Least Mean Square (LMS) algorithm and estimates the weights of a Fourier series of a periodic signal [12]. The FLC works with an adaptive step μ and the adaptive weights are updated according to Equations (7)-(9).

$$x_{rk} = \begin{cases} \sin(r\omega_0 k), 1 \le r \le M \\ \cos\big((r-M)\omega_0 k\big), M+1 \le r \le 2M \end{cases} \quad (7)$$

$$\varepsilon_k = s_k - W_k X_k \quad (8)$$

$$W_{k+1} = W_k + 2\mu X_k \varepsilon_k \quad (9)$$

Where W_k is the adaptive weight vector, X_k is the vector of x_{rk}, M is the number of harmonics in the model, r is the harmonic index, ε_k is the system deviation, and s_k is the input signal for a k sample. The number of harmonics M to be extracted from the measured signal defines the size of the W_k and x_{rk} vectors.

Weighted-Frequency Fourier Linear Combiner (WFLC) [13] allows the tracking of the highest magnitude component present in the periodic signal and can readjust its frequency. This adaptation is achieved using a modified LMS algorithm, shown in Equation (10).

$$\omega_{0_{k+1}} = \omega_{0_k} + 2\mu_0\varepsilon_k \sum_{r=1}^{M} r\left(\omega_{r_k} x_{(M+r)_k} - \omega_{(M+r)_k} x_{r_k}\right) \qquad (10)$$

Where ω_0 is the frequency of the greater magnitude component and μ_0 is the adaptive step for the modified LMS.

The combination of FLC and WFLC algorithms can track the amplitude, phase, and frequency of periodic signals. In combined FLC and WFLC applications, it is common to use the WFLC only to adjust the frequency. The block diagrams of FLC and WFLC algorithms are shown in Fig. 2.

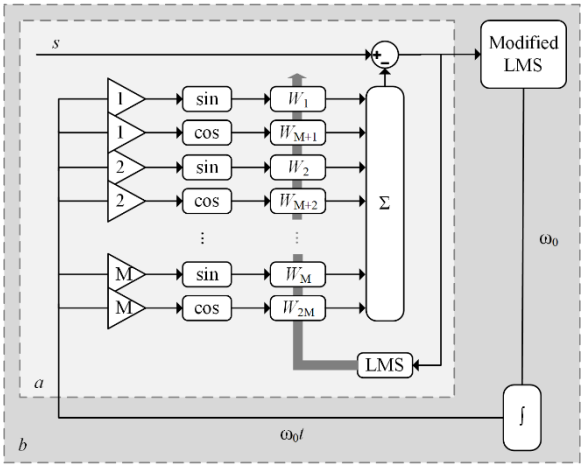

Fig. 2 - Fourier linear combiners algorithms: (a) Original FLC and (b) WFLC

The three-phase weighted-frequency Fourier linear combiner (3WFLC) is an improvement of the FLC algorithm and is applied in three-phase systems. In the 3WFLC algorithm, the adaptive frequency ω_0 is the average of the frequencies obtained by the WFLC algorithm in each phase.

The combination of one 3WFLC and three FLC can be used to decompose three-phase periodic signals into a Fourier series. From the decomposed signal, a Fortescue transform is used to determine the positive, negative, and zero sequences of each harmonic component tracked by the FLCs. This structure is the sequence detector Fourier linear combiner (SDFLC) [14]. The 3WFLC/SDFLC [15] block diagram is shown in Fig. 3. From the signal decomposed by the 3WFLC/SDFLC, it is possible to choose which harmonic orders and sequences of the signal will be compensated and a different controller can be applied to each component to mitigate the selected harmonic.

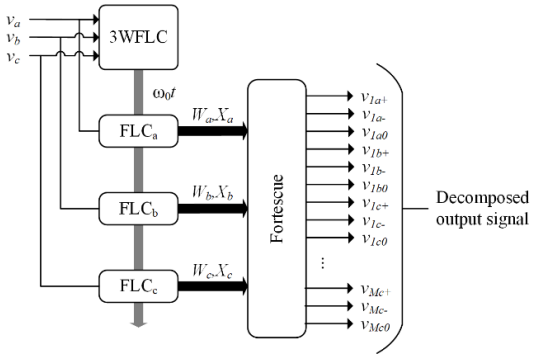

Fig. 3 - 3WFLC/SDFLC block diagram

IV. Proposed Adaptative Harmonic Mitigation

In the proposed work, an adaptive gain k_{v5_k} was defined for the 5th harmonic order, a gain k_{v7} for the 7th harmonic order, a k_{v11} gain for the 11th, and a k_{v13} gain for the 13th harmonic order. The update time (T_u) of the adaptive gain is 200 ms, which is the time window usually used in harmonic measurements [16] and this gain is adjusted according to the error between the average values of the 5th voltage harmonic in a bus of interest in the system (v_{5_k} e $v_{5_{(k-1)}}$, respectively) and the current that feeds this bus (i_{5_k} e $i_{5_{(k-1)}}$, respectively) at instants k and $k-1$. The voltage v_5 is the average of the instantaneous 5th harmonic order voltages on the bus and the current i_5 is the average of the instantaneous harmonic currents that feed the bus, as shown in (11) e (12).

$$|v_g|_{h=5} = (v_{a5} + v_{b5} + v_{c5})/3 \qquad (11)$$

$$|i_g|_{h=5} = (i_{a5} + i_{b5} + i_{c5})/3 \qquad (12)$$

Where v_{a5}, v_{b5}, and v_{c5} are the 5th harmonic voltages and i_{a5}, i_{b5} and i_{c5} are the 5th harmonic currents in a bus of interest in the system.

The average values of the 5th harmonic order voltage on a bus of interest in the system (v_{5_k}) and the current that feeds this bus (i_{5_k}) are calculated in a time window of 200 ms.

The adaptive gain of the proposed strategy is given by (13).

$$k_{v5_k} = k_{v5_{(k-1)}} - \Delta k_{v5}.\varepsilon_{v5} - \Delta k_{i5}.\varepsilon_{i5} \qquad (13)$$

Where Δk_{v5} is the gain voltage step, Δk_{i5} is the gain current step, and $k_{v5_{(k-1)}}$ is the adaptive gain at the instant $k-1$, ε_{v5} and ε_{i5} are the voltage and current deviations at instants two consecutives instants $(v_{5_k} - v_{5_{(k-1)}})$ and $(i_{5_k} - i_{5_{(k-1)}})$, respectively.

The adaptive gain of the proposed strategy tries to minimize the 5th harmonic order voltage and current harmonics on a bus of interest in the system. Fig. 4 shows the flowchart of the harmonic detector based on FLC with adaptive gain proposed in this work.

The adaptive gain is limited in order to guarantee the stable operation of the harmonic controller. The minimum gain value is represented by k_{v5MIN} and the maximum value by k_{v5MAX} in Fig. 4.

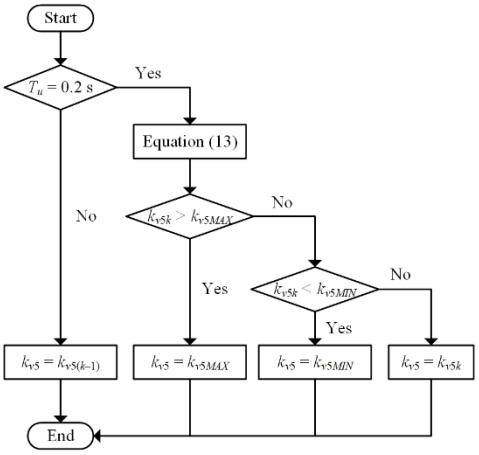

Fig. 4 - Flowchart of the gain adjustment of the harmonic detector FLC-based with adaptive gain

Harmonic current reference is given by (14).

$$i_h^* = \sum_{h=5,7,11,13} k_{vh} \, . \, v_{h,p} \qquad (14)$$

Where k_{vh} is the h^{th} harmonic order gain and $v_{h,p}$ is the phase p h^{th} harmonic order voltage. This strategy aims to dampen the system harmonic voltages ($v_{h,p}$) through a local current harmonic compensation (i_h^*).

V. Stability Discussion

Stability analysis studies of various VSG implementations are presented in [17] and [18]. According to these articles, a current-controlled virtual synchronous machine (CCVSM), similar to the VSG implemented in this article, has good inherent characteristics in terms of stability [17] and the eigenvalue analysis also showed that it is more influenced by the control parameters and has the highest stability margins among the studied approaches [18].

Regarding active power filters, [19] and [20] present stability analysis studies of three types of harmonic compensation methods commonly used in active filters. In terms of stability, the control strategy based on voltage detection, that is used in this work, is the most suitable for active parallel filters [19].

Some articles that propose combining VSG control with harmonic compensation [4][5][7][8] present stability analysis studies that demonstrate that the combination of these controls can be stable.

These papers show that VSG and harmonic compensation controls, when used together or separately, can be stable. A stability analysis study of the proposed control in this paper will be developed in future work.

VI. Results

In this section, two inverters using the proposed detection strategy are applied in a four-bar system. The converter and grid/load system will be simulated in real-time in Hardware-in-the-Loop (HIL) Typhoon HIL404 module. Texas Instruments' digital signal processor TMSF28379D was used to implement the VSG and harmonic detection controls. The signals shown in this section were captured using the HIL SCADA from Typhoon HIL Control Center toolchain. Fig. 5 shows the HIL bench used to obtain the results.

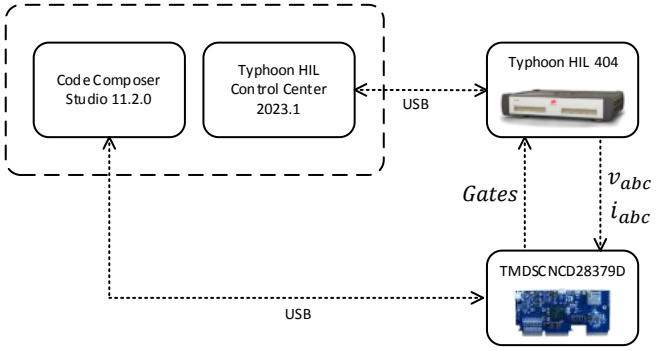

Fig. 5 - HIL test-bench used for real time simulation

Fig. 6 shows the overview of the simulated system with four buses. The proposed circuit is simulated in Typhoon HIL Control Center environment. Inverters are connected to buses 3 and 4 and two non-linear loads are connected to buses 2, 3, and 4. Based on measurements of the voltage on bus 2 (v_g) and the feeder current (i_g), the inverter controllers connected to buses 3 and 4 act to dampen the 5th harmonic order voltage on bus 2. The grid voltage source consists of an inertial voltage source with a 0.05 pu 5th harmonic which represents the harmonic distortion present in a distribution system due to the circulation of harmonic currents in the feeders. The renewable energy source (RES) is emulated by a DC voltage source (V_{DC}) and is connected to the grid through a three-phase inverter, which, in turn, is connected to the system through an LCL filter. The inverter switches are IGBTs with anti-parallel diodes connected across and the current controller is a proportional integral-resonant (PI-RES) controller [21]. The simulated system has three loads: load 1 is a three-phase rectifier with a RL load; load 2 is composed of a single-phase rectifier with a RL load connected between phases *a* and *b*, a single-phase RL load connected between phases *a* and *c*, and a single-phase RL load connected between phases *b* and *c*; and load 3 is a balanced three-phase RL load. In the simulation, load 1 is always connected to the system, load 2 is connected at $0 < t < 2$ s, and load 3 is connected at $t > 3$ s. Load 1 is connected to bus 4 and loads 2 and 3 are connected to bus 2. The inertial grid, distribution system and VSG parameters are shown in Table I, the parameters used for the design of the LCL filter, designed according to [22] are shown in Table II, PI-RES controller gains are shown in Table III, and active and reactive powers of the loads are shown in Table IV. To verify the adaptive gain behavior, the system load was changed in two moments. Fig. 7 shows the inertial grid diagram. In Fig. 7, H_{eq} is the inertia, R is the droop gain, p_{g0} is the reference electrical power, ω_b is the base angular velocity, ω_e is the angular velocity, θ_e is the grid angle, and V_e is the voltage magnitude. For the results presented in this section, the VSG control references are $P^* = 0$ and $Q^* = 0$.

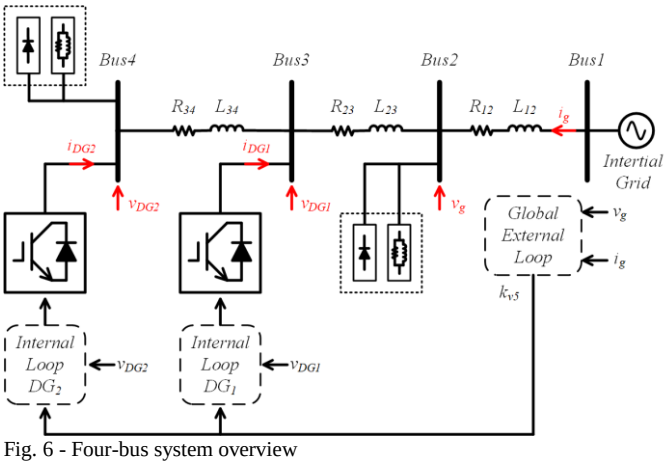

Fig. 6 - Four-bus system overview

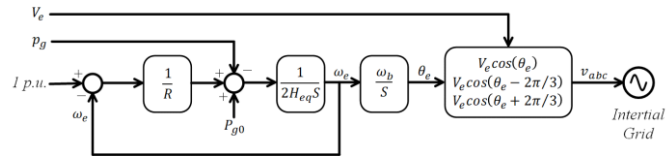

Fig. 7 - Inertial grid voltage source

TABLE I
INERTIAL GRID, DISTRIBUTION SYSTEM AND VSG PARAMETERS

Parameter	Value
Inertial grid voltage magnitude (V_e)	179.6051 V
Inertial grid base power (S_b)	500.0 kW
Inertial grid base angular velocity (ω_b)	376.9911 rad/s
Grid inertia (H_{eq})	5.0 s
Grid droop coefficient (R)	0.0002
Grid reference active power (p_{g0})	1.0 p.u.
Line resistance, section 12 (R_{s12})	0.02 Ω
Line inductance, section 12 (L_{s12})	0.18 mH
Line resistance, section 23 (R_{s23})	0.05 Ω
Line inductance, section 23 (L_{s23})	0.18 mH
Line resistance, section 34 (R_{s34})	0.05 Ω
Line inductance, section 34 (L_{s34})	0.18 mH
DC-link voltage (V_{DC})	500.0 V
VSG resistance (R_{VSG})	0.05 Ω
VSG inductance (L_{VSG})	0.32239 mH
VSG moment of inertia (J)	0.3 kg.m²
VSG damping coefficient (D)	20.0
VSG droop coefficient (D_p)	200.0

TABLE II
LCL FILTER SPECIFICATION AND PARAMETERS

Parameter	Value
Switching frequência (f_s)	10 kHz
Grid frequency (f_n)	60 Hz
Converter rated power (P_n)	50 kW
Source ph-ph voltage (E)	220 V
Current ripple (ΔI)	5 %
Reactive power absorbed under rated conditions (x)	5 %
Inverter side inductance (L_1)	0.27944 mH
Grid side inductance (L_f)	0.04295 mH
Capacitance (C_f)	137.01 µF
Resistance (R_d)	0.75 Ω

TABLE III
PI-RES CONTROLLER GAINS

Parâmetros	Value
Proportional gain (K_p)	1.0
Integral gain (K_i)	50.0
Resonant gain (K_r)	25.0

TABLE IV
LOADS ACTIVE AND REACTIVE POWERS AND THD

Load	Type	P_L (kW)	Q_L (kvar)
1	3ph rectifier	26.85	-
2	1ph rectifier	8.91	-
	RL	3.39	1.67
	RL	2.62	0.9
3	3ph balanced RL	4.30	4.10

A. Adaptive harmonic damping contribution

This simulation shows the behavior of adaptive gain in a scenario where there is load change at t = 2 s and t = 3 s. The controller gains are k_{v7} = 2.0 and k_{v11} = k_{v13} = 1.0. Adaptive gain k_{v5} has initial gain k_{v5} = 0.5, voltage step gain Δk_{v5} = 0.4, current step gain Δk_{i5} = 0.3, minimum gain value k_{v5MIN} = 0.5, and maximum gain value k_{v5MAX} = 3.5.

The profile of the 5th harmonic voltages and currents of the feeder on bus 2 and the k_{v5} adaptive gain are shown in Fig. 8.

As can be seen in Fig. 8, at t = 0.0 s the adaptive gain is activated. At t = 0.4 s the gain is updated and the 5th order harmonic voltage and current of bus 2 are reduced. At t = 0.6 s, the gain is updated again and reduces the 5th order harmonic current and the 5th order harmonic voltage does not change significantly. From t = 0.8 s, changing the adaptive gain value does not significantly change the 5th order harmonic voltage and current on bus 2. From t = 0.8 s, the difference between the voltages measured at instants k and $k-1$ (v_{5_k} and $v_{5_{(k-1)}}$, respectively) decreases and the adaptive gain k_{v5} tends to stabilize. Although the voltage stabilizes, changing the load causes the gain to change slightly at t = 2.0 s and t = 3.0 s. At t = 2.0 s, the error between the currents measured at times k and $k-1$ (i_{5_k} and $i_{5_{(k-1)}}$, respectively) decreases, causing the adaptive gain to increase. At t = 3.0 s, the error between i_{5_k} e $i_{5_{(k-1)}}$ increases, causing the adaptive gain to decrease.

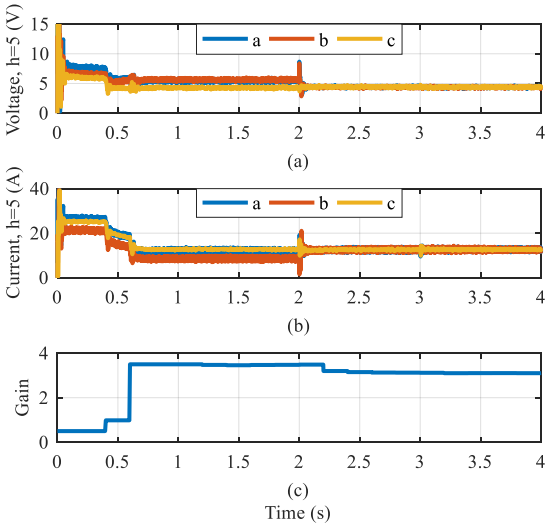

Fig. 8 – Amplitude of 5th harmonic (a) voltages and (b) currents on bus 2 and (c) the k_{v5} adaptive gain

Fig. 9, 10, and 11 show the voltages on buses 2, 3, and 4 at intervals at three different times. The use of a harmonic voltage damping strategy can significantly mitigate voltage distortion on buses 2, 3, and 4, as seen in the Fig. 9, 10, and 11.

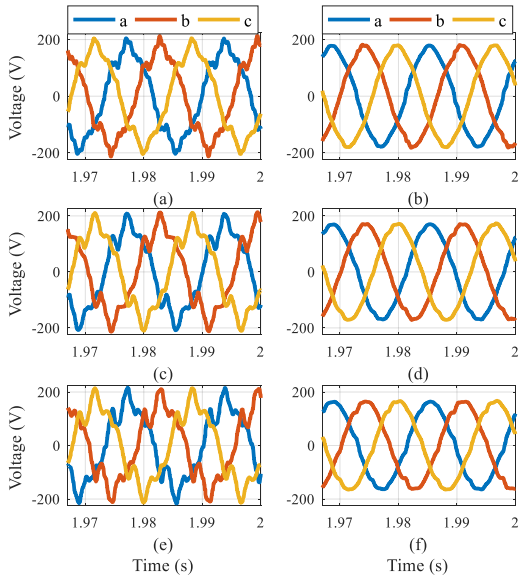

Figure 9 - Voltage on bus 2 (a) without and (b) with compensation; voltage on bus 3 (c) without and (d) with compensation; and voltage on bus 4 (e) without and (f) with compensation at *t* = 2 s

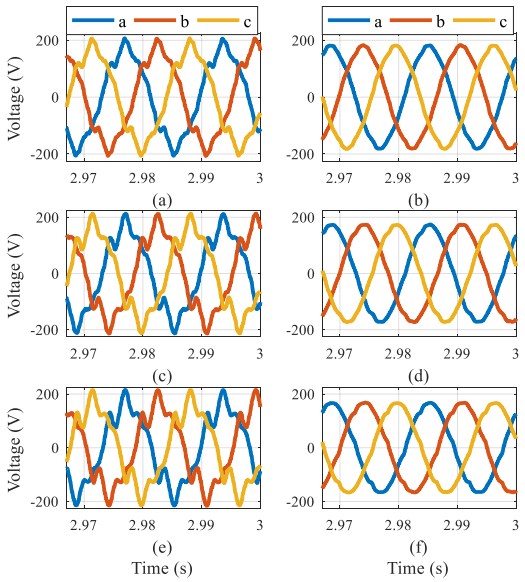

Fig. 10 - Voltage on bus 2 (a) without and (b) with compensation; voltage on bus 3 (a) without and (b) with compensation; and voltage on bus 4 (a) without and (b) with compensation at t = 3 s

Table V shows the individual harmonic distortions (IHD) and THD of the voltages on buses 2, 3, and 4 before and after the compensation and the limits established by the IEEE Std 519-2022 [23]. Before compensation, the 5th and 7th order IHDs and the THD on the three phases of the three buses analyzed are above the limits established in the standard. With compensation, these values are within the values established in the standard and the other IHDs and THDs have their values reduced, as shown in Table V.

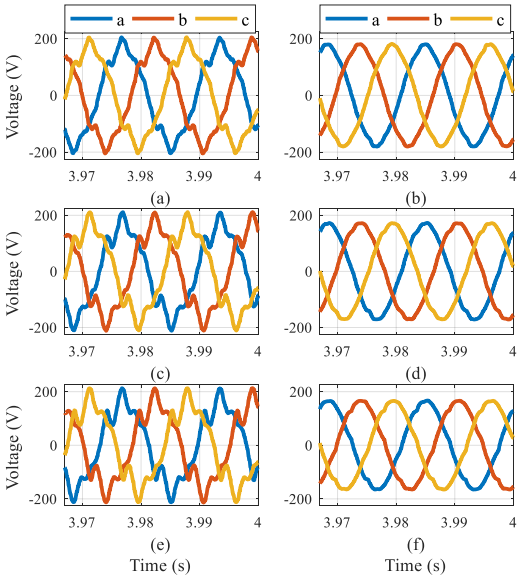

Fig. 11 - Voltage on bus 2 (a) without and (b) with compensation; voltage on bus 3 (c) without and (d) with compensation; and voltage on bus 4 (e) without and (f) with compensation at t = 4 s

TABLE V
IHDS AND THDS OF VOLTAGES ON BUSES 2, 3, AND 4 WITHOUT AND WITH COMPENSATION

***t*(s)**	**Bus**	***h***	**w/o comp. (%)**			**w/ comp. (%)**			**IEEE 519**
			a	**B**	**c**	**a**	**b**	**c**	
2	2	5	10.1	10.4	9.2	2.8	2.6	2.5	5.0
		7	6.1	6.5	5.8	0.1	0.1	0.1	5.0
		THD	12.4	13.2	11.2	3.0	3.0	2.9	8.0
	3	5	14.1	15.0	14.2	1.5	1.1	1.0	5.0
		7	11.5	11.7	10.6	0.8	1.3	1.3	5.0
		THD	19.0	19.6	17.9	2.4	2.7	2.2	8.0
	4	5	17.8	19.0	18.2	2.1	2.2	2.2	5.0
		7	15.2	15.2	13.7	1.7	1.6	1.0	5.0
		THD	23.8	24.7	23.0	3.5	3.8	3.2	8.0
3	2	5	9.9	9,.2	9.5	2.5	2.2	2.2	5.0
		7	5.6	6.4	6.2	0.4	0.7	0.7	5.0
		THD	11.7	11.5	11.7	2.9	2.5	2.5	8.0
	3	5	14.3	14.1	14.5	0.8	1.4	0.9	5.0
		7	10.8	10.8	9.8	1.1	1.2	0.5	5.0
		THD	18.4	18.2	17.9	2.5	2.4	2.0	8.0
	4	5	18.0	18.3	18.1	2.1	1.8	2.1	5.0
		7	14.6	14.3	14.2	1.5	1.1	1.6	5.0
		THD	23.5	23.5	23.2	3.2	2.5	3.3	8.0
4	2	5	9.3	9.6	9.6	2.2	2.2	2.7	5.0
		7	6.0	5.7	5.9	0.8	0.9	0.2	5.0
		THD	11.5	11.5	11.5	2.4	2.6	3.1	8.0
	3	5	13.7	13.9	14.4	1.7	1.1	1.2	5.0
		7	11.4	11.3	10.6	1.4	1.6	1.0	5.0
		THD	18.2	18.3	18.3	3.0	2.8	2.2	8.0
	4	5	17.2	17.4	17.9	1.4	1.9	2.0	5.0
		7	14.6	14.6	14.0	2.1	1.4	1.9	5.0
		THD	22.8	23.0	23.0	3.2	3.0	3.5	8.0

Table VI shows the IHDs and THD of the feeder currents of sections 12, 23, and 34 before and after compensation and the limits established by the IEEE Std 519-2022. Before compensation, the 5th order IHDs and 7th order IHDs on sections 12 and 23 are above the limits established in the IEEE Std 519-2022. With harmonic compensation, IHDs and THDs decrease and, in some cases, stay within the limits established by the standard. The 7th order IHD on sections 12, 23, and 34

stay within the limits proposed by the standard. As this harmonic detection strategy aims to dampen the voltage harmonics present in the electrical system, the mitigation of harmonic currents in the feeders is not as efficient as the damping of harmonic voltage propagation.

TABLE VI
IHDS AND THDS OF CURRENTS ON FEEDERS 12, 23, AND 34 WITH AND WITHOUT COMPENSATION

t(s)	Sec.	*h*	w/o comp. (%)			w/ comp. (%)			IEEE 519
			a	b	c	a	b	c	
2	12	5	17.1	19.6	18.7	7.3	6.5	10.5	7.0
		7	12.3	14.6	14.6	0.6	1.9	1.4	7.0
		THD	21.2	24.5	23.9	7.4	7.0	10.7	8.0
	23	5	17.3	19.9	19.9	15.3	16.5	12.8	4.0
		7	14.8	12.9	12.7	3.1	3.1	1.1	4.0
		THD	23.2	24.4	23.9	15.7	16.8	12.9	5.0
	34	5	7.0	9.1	9.1	2.9	3.6	2.6	4.0
		7	2.0	0.4	1.9	3.3	2.6	4.2	4.0
		THD	10.4	11.5	11.2	4.8	5.0	5.7	5.0
3	12	5	28.6	28.8	28.3	13.2	13.4	13.7	7.0
		7	22.0	22.7	22.0	1.9	1.9	1.5	7.0
		THD	36.2	36.9	36.0	13.5	13.5	13.8	8.0
	23	5	19.5	19.1	19.3	12.3	13.0	13.0	4.0
		7	12.6	13.0	12.7	1.8	1.2	1.2	4.0
		THD	23.4	23.3	23.4	12.6	13.1	13.1	5.0
	34	5	8.8	8.8	9.0	2.9	2.5	2.4	4.0
		7	1.7	1.6	2.0	3.6	4.1	3.8	4.0
		THD	10.8	10.8	10.9	5.1	5.5	5.2	5.0
4	12	5	22.5	22.5	22.8	11.3	12.0	12.4	7.0
		7	17.6	17.9	18.1	1.1	0.6	1.3	7.0
		THD	28.7	28.9	29.2	11.4	12.1	12.5	8.0
	23	5	19.9	19.2	19.4	13.3	13.0	12.9	4.0
		7	13.2	12.8	12.7	1.2	1.0	0.7	4.0
		THD	24.2	23.3	23.5	13.4	13.1	12.9	5.0
	34	5	9.3	8.6	9.1	3.2	2.8	3.6	4.0
		7	2.2	1.6	2.1	2.8	3.7	3.7	4.0
		THD	11.4	11.0	11.0	5.1	5.2	5.8	5.0

B. *Virtual inertia contribution*

To verify that the proposed control combination can contribute to improving the frequency and ROCOF (rate of change of frequency) of the system, two simulations were done to compare the contribution of the constant PQ control based on *p-q* Theory [24] and the VSG control combined with the harmonic detection strategy proposed in this article. For the results presented in this section, the VSG control references are $P^* = 10$ kW and $Q^* = 0$.

Fig. 12 shows DG1 and DG2 active power, the frequency, and the ROCOF on buses 2, 3, and 4 for combinations of the proposed detection strategy with constant PQ and VSG controls. Table VI shows the frequencies and ROCOFs after the transients at $t = 2$ s and $t = 3$ s, respectively.

The ROCOF is given by (15) [25].

$$ROCOF(t) = \frac{df(t)}{dt} = \frac{f(t) - f(t - T_s)}{T_s} \qquad (15)$$

Where T_s is the sampling time.

In simulations, the sampling time for ROCOF calculation is 0.1 ms and the average ROCOF is calculated in a window of 0.1 s [26]. Comparing Fig. 12 (a) and (d), while the PQ control keeps the active power practically constant during transients, the VSG control injects a flow of active power into the system at these moments. With the variation of the system frequency, a variation of the angular velocity would be observed, causing the inverter to inject an active power flow into the system to compensate for the momentary unbalance.

As seen in Table VII, the VSG control can reduce the peaks of the oscillations that happen at instants $t = 2$ s and $t = 3$ s. Thus, it was possible to verify that the VSG control can contribute to the improvement of the frequency nadir and the ROCOF in the PCC.

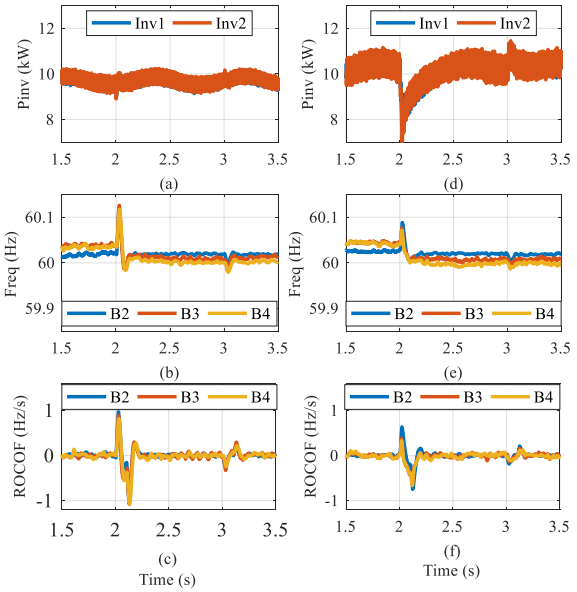

Fig. 12 - (a) DG1 and DG2 active powers, (b) frequency, and (c) ROCOF on the buses 2, 3, and 4 with the application of the combination of PQ control with the proposed detection strategy and (d) DG1 and DG2 active powers, (e) frequency, and (f) ROCOF on the buses 2, 3, and 4 with the application of the combination of VSG control with the proposed detection strategy

TABLE VII
FREQUENCY AND ROCOF VALUES DURING TRANSIENTS USING PQ AND VSG CONTROLS

t (s)	Ctrl	Bus	Freq (Hz)		ROCOF (Hz/s)	
			Min.	Max	Min.	Max.
2	PQ	2	59.99	60.11	–1.02	0.97
		3	59.99	60.13	–1.08	0.89
		4	59.98	60.12	–1.08	0.82
	VSG	2	60.01	60.09	–0.75	0.63
		3	60.00	60.08	–0.65	0.38
		4	60.00	60.07	–0.67	0.33
3	PQ	2	59.99	60.02	–0.25	0.25
		3	59.98	60.02	–0.33	0.30
		4	59.98	60.01	–0.25	0.22
	VSG	2	60.00	60.02	–0.19	0.21
		3	59.99	60.01	–0.14	0.16
		4	59.99	60.00	–0.12	0.12

VII. CONCLUSIONS

This article proposes a control that combines the features of the VSG control with an FLC-based harmonic detector with adaptive gain. With the proposed control, a single inverter can simultaneously contribute the system stability and power quality improvement. The adaptive gain is adjusted according to the error of the 5th harmonic order voltages and currents of a bus of interest in the grid. Simulations in a four-bus system

using the Typhoon HIL Control Center toolchain were done to show that the combination of the VSG and the FLC-based voltage harmonic detection with adaptive gain can simultaneously improve system stability and power quality across the grid

From the data shown in Tables V and VI, the proposed controller can reduce the voltages and harmonic currents of the system and, thus, improve the system power quality. In some cases, the harmonics are within the limits proposed by the IEEE Std 519-2022, after harmonic compensation. Fig. 6 shows that the adaptive gain stabilizes after transients.

Table VII shows that the VSG control can reduce the peaks of the frequency oscillations and improve the ROCOF after the transients at $t = 2$ s and $t = 3$ s, and thus contribute to the system stability.

VIII. Acknowledgment

This work was supported by the "10 for 10 Typhoon HIL Awards Program."

IX. References

[1] G. Pepermans, J. Driesen, D. Haeseldonckx, R. Belmans, and W. D'haeseleer, "Distributed generation: definition, benefits and issues," *Energy Policy*, vol. 33, issue 6, pp. 787-798, Apr. 2005.

[2] L. F. Encarnação, D. Carletti, S. A. Souza, O. Barros Jr., D. C. Broedel, and P. T. Rodrigues, "11 – Virtual Inertia for Power Converter Control," in *Advances in Renewable Energies and Power Technologies*, I. Yahyaoui, Elsevier, 2018, pp. 377-411.

[3] L. Morán, J. Dixon, "Active Filters," in *Power Electronics Handbook*, 2nd ed., M.H. Rashid (Ed.), Academic, Burlington, 2006, pp. 1067-1102.

[4] Z. Qu, H. Yang, Y. Cai, and H. Wang, "Application of virtual synchronous generator technology in three-phase four-leg inverter," in *Proc. 2017 20th International Conference on Electrical Machines and Systems (ICEMS)*, 2017, pp. 1-6.

[5] H. M. Kazemi, E. Afjei, and A. Rahmati, "A Combination of VSG and Amended Fractional-Order Repetitive Control for Improving Power Quality of Grid-Connected Inverter," in *Proc 2019 20th International Scientific Conference on Electric Power Engineering (EPE)*, 2019, pp. 1-6.

[6] T. S. Amorim, D. Carletti, and L. F. Encarnação, "Comparison of inverter controllers with synthetic inertia and harmonic compensation features," *Electric Power Systems Research*, vol. 197, pp. 107344, Aug. 2021.

[7] G. Lou, Q. Yang, W. Gu, X. Quan, J. M. Guerrero, and S. Li, "Analysis and Design of Hybrid Harmonic Suppression Scheme for VSG Considering Nonlinear Loads and Distorted Grid," *IEEE Transactions on Energy Conversion*, vol. 36, no. 4, pp. 3096-3107, Dec. 2021.

[8] B. W. França, M. Aredes, L. F. d. Silva, G. F. Gontijo, T. C. Tricarico, and J. Posada, "An Enhanced Shunt Active Filter Based on Synchronverter Concept," *IEEE Journal of Emerging and Selected Topics in Power Electronics*, vol. 10, no. 1, pp. 494-505, Feb. 2022.

[9] D. Hosseini, M. Naderi, Q. Shafiee, M. Savaghebi, and H. Bevrani, "Virtual Synchronous Generator Controller for Power Quality Enhancement in Microgrids," in *Proc. 2022 8th International Conference on Control, Instrumentation and Automation (ICCIA)*, 2022, pp. 1-6.

[10] Y. Chen, R. Hesse, D. Turschner and H. -P. Beck, "Improving the grid power quality using virtual synchronous machines," in *Proc. 2011 International Conference on Power Engineering, Energy and Electrical Drives*, 2011, pp. 1-6.

[11] P. Kundur, N. J. Balu, and M. G. Lauby. *Power System Stability and Control*, 1st. ed, New York: McGraw-Hill, 1994.

[12] C. Vaz, X. Kong and N. Thakor, "An adaptive estimation of periodic signals using a Fourier linear combiner," *IEEE Transactions on Signal Processing*, vol. 42, no. 1, pp. 1-10, Jan. 1994.

[13] C. N. Riviere and N. V. Thakor, "Modeling and canceling tremor in human-machine interfaces," *IEEE Engineering in Medicine and Biology Magazine*, vol. 15, no. 3, pp. 29-36, May-June 1996.

[14] C. N. Riviere, R. S. Rader, and N. V. Thakor, "Adaptive cancelling of physiological tremor for improved precision in microsurgery," *IEEE Transactions on Biomedical Engineering*, vol. 45, no. 7, pp. 839-846, July 1998.

[15] O. Barros Jr., T. S. Amorim, D. Carletti, A. Frizera Neto, and L. F. Encarnação, "Design of an Enhanced FLC-Based Controller for Selective Harmonic Compensation in Active Power Filters," *Electronics*, vol. 9, no. 12, pp. 2052, Dec. 2020.

[16] *IEEE Recommended Practice for Monitoring Electric Power Quality*, IEEE Std 1159-2019 (Revision of IEEE Std 1159-2009), pp.1-98, 13 Aug. 2019.

[17] E. Unamuno, A. Rygg, M. Amin, M. Molinas and J. A. Barrena, "Impedance-Based Stability Evaluation of Virtual Synchronous Machine Implementations in Converter Controllers," in *Proc. 2018 International Power Electronics Conference (IPEC-Niigata 2018 -ECCE Asia)*, pp. 759-766.

[18] E. Unamuno, J. A. Suul, M. Molinas and J. A. Barrena, "Comparative Eigenvalue Analysis of Synchronous Machine Emulations and Synchronous Machines," in *Proc. IECON 2019 - 45th Annual Conference of the IEEE Industrial Electronics Society*, pp. 3863-3870.

[19] H. Akagi, "Control strategy and site selection of a shunt active filter for damping of harmonic propagation in power distribution systems," *IEEE Transactions on Power Delivery*, vol. 12, no. 1, pp. 354-363, Jan. 1997.

[20] H. Fujita, T. Yamasaki and H. Akagi, "A hybrid active filter for damping of harmonic resonance in industrial power systems," *IEEE Transactions on Power Electronics*, vol. 15, no. 2, pp. 215-222, March 2000.

[21] M. Liserre, R. Teodorescu, and F. Blaabjerg, "Multiple harmonics control for three-phase grid converter systems with the use of PI-RES current controller in a rotating frame," *IEEE Transactions on Power Electronics*, vol. 21, no. 3, pp. 836-841, May 2006.

[22] M. Liserre, F. Blaabjerg, and S. Hansen, "Design and control of an LCL-filter-based three-phase active rectifier," *IEEE Transactions on Industry Applications*, vol. 41, no. 5, pp. 1281-1291, Sept.-Oct. 2005.

[23] *IEEE Standard for Harmonic Control in Electric Power Systems*, IEEE Std 519-2022 (Revision of IEEE Std 519-2014), pp.1-31, 5 Aug. 2022.

[24] H. Akagi, E.H. Watanabe, M. Aredes, *Instantaneous Power Theory and Applications to Power Conditioning*, John Wiley & Sons, New Jersey, 2007. IEEE Press Series on Power Engineering.

[25] M. W. Altaf, M. T. Arif, S. Saha, S. N. Islam, M. E. Haque, and A. M. T. Oo, "Effective ROCOF-Based Islanding Detection Technique for Different Types of Microgrid," *IEEE Transactions on Industry Applications*, vol. 58, no. 2, pp. 1809-1821, March-April 2022.

[26] *IEEE Standard for Interconnection and Interoperability of Distributed Energy Resources with Associated Electric Power Systems Interfaces*, IEEE Std 1547-2018 (Revision of IEEE Std 1547-2003), pp.1-138, 6 April 2018.